

Model of Loaded Contact in Multi-pair Gears

E. Trubachev, A. Kuznetsov and A. Sannikov

Abstract The paper describes the problem of LTCA of a heavy-loaded multi-pair spiroid gear. The algorithm for analysis of load distribution, accounting for elastic and elastic-and-plastic contact in general and micro-roughnesses of contact surfaces in particular, is proposed. Agreement of the algorithm at various accelerating procedures is studied. Numerical examples that illustrate the efficiency of the algorithm are given.

Keywords LTCA · Multi-pair heavy-loaded gear · Elastic and plastic contact

1 Introduction

It became common in both the theory and practice of gearing [4, 5, 8] to solve the problems of assessing the load state and strength with account for the elastic character of contact interaction. The traditional means of solution of this problem is the finite element method (FEM) and the corresponding software. The following inter-related problems of FEM application for analysis of loaded gears should be mentioned:

- increase in error of computations for cases of assessing the stresses at tooth roots for relatively non-smooth conjugations between tooth flanks and their roots;
- abrupt increase in the computational complexity (requirements for computational resources, accumulation of computational error because of rounding at numerous operations, provision of convergence) for the case of a multi-pair contact.

The assessment of stresses at tooth roots of multi-pair spiroid gears should be related to these exact cases. As for gears of heavy-loaded, low-speed gearboxes, the calculation values reach 1500–2000 MPa, even for maximum contact stresses that

E. Trubachev (✉) · A. Kuznetsov · A. Sannikov
Kalashnikov Izhevsk State Technical University, Izhevsk, Russia
e-mail: truba@istu.ru

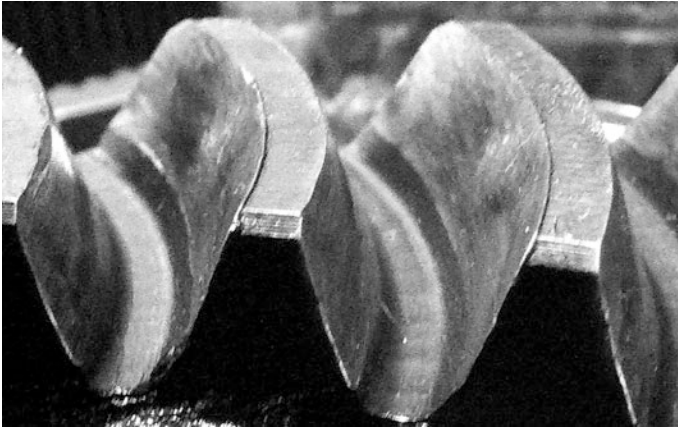


Fig. 1 Crumbling of apexes of spiroid gearwheel teeth after heavy loading

are uniformly distributed along lines of the conjugated contact. Concern over loss of contact and/or the bending strength of teeth at stress concentration in these or those areas due to the action of errors and deformations is natural. However, these gears do successfully operate. Evidently, this is due to the rapid equalizing of loads acting on teeth and to the reduction of corresponding stresses. The practice of testing and operation proves this assumption: even after the first cycles of heavy loading, one can observe plastically deformed areas of teeth (Fig. 1). Therefore, consideration of this factor is very urgent for assessment of the strength of multi-pair heavy-loaded spiroid gears.

As for the elastic-and-plastic statement of the problem, the above-mentioned issues of FME application are revealed to an even greater extent. For this reason, we developed the original iterative algorithm of analysis of the elastic and elastic-and-plastic loaded contact in the spatial multi-pair gear; the present paper considers its basic aspects.

2 Model of the Elastic Loaded Contact

As usual, let us consider that such an initial position of gear elements (accounting for errors) is determined before the analysis, at which time the clearance between teeth at a certain point or points is equal to zero (the presence or absence of the common normal at this point is insignificant). At the remaining points of the flanks, there is a clearance S_0 that is greater than zero.

As is known, the loaded gear is a multiply statically indeterminable system with unilateral links. As for the discretized representation of this system, the following conditions should be fulfilled for cells of tooth flanks that participate in the load transmission:

$$\begin{cases} \sum_D F_{k'm'} v_{km k'm'} + S_{0km} - \Delta_{\varphi 2km} = 0; \\ \sum_D F_{k'm'} \check{r}_{2k'm'} - T_2 = 0; \end{cases} \quad (1)$$

where S_{0km} is the initial (prior to load application) clearance between the km th cells of surfaces for the position of links when the clearance at one of the cells is equal to zero, $v_{km k'm'}$ is the value of the influence function determining the transmission of surfaces at the km th cells when applying the unit loads at the $k'm'$ th cells, $\Delta_{\varphi 2km}$ is the relative transmission of the km th cells as a result of the close approach of elements at gear loading, and $\check{r}_{2k'm'}$ is the arm of action of the force $F_{k'm'}$ applied at the $k'm'$ th knot with respect to the gearwheel axis. The first km equations of system (1) are the conditions of compatibility for the displacement of points of contacting areas of teeth (in the model, they are the cells of the contact area), the latter equation is the equation of equilibrium of torques developed by forces applied at cells and the external torque T_2 applied to the gearwheel.

The cells at which forces are applied are unknown prior to analysis; therefore, neither the number of the first km equations of system (1), nor their specific form are known either. That is why iterative algorithms of calculation [1, 2, 11, 12] were given development implying the consequent specification of: the approaching of elements, the contact area, and the values of discretely applied forces. The latter for the elastic statement linearly influence the displacement of tooth points (by the factors $v_{km k'm'}$).

Our developed algorithm for solving system (1) originated in works by Zablonksy [13] and Sheveleva [11]; and it implied the following steps (see also Fig. 2):

- (1) *The value of the initial approach of elements is assigned as $\Delta\varphi_2^{(n)} = \Delta\varphi_2^{(1)}$ (here and further within description of the algorithm, n is the number of the iteration). The result is the formation of the area $D^{(1)}$ with the penetration of teeth into each other.*
- (2) *For the pointed area, the zero approach of discretely applied forces is determined as $F_{km}^{(n)} = F_{km}^{(1)}$ with account for the condition of force equilibrium proportional to the formed penetrations $S_{0km} - \Delta_{\varphi 2km}^{(1)}$ as follows:*

$$f_{km}^{(1)} = S_{0km} - \Delta_{\varphi 2km}^{(1)}, \quad (2)$$

$$F_{km}^{(1)} = T_2 f_{km}^{(1)} / \sum_D f_{km}^{(1)} \check{r}_{2km} \quad (3)$$

The following steps of the algorithm are related to both the first and all the subsequent n th iterations.

- (3) *Displacement of points due to application of forces and corresponding discrepancies ξ_{km} of the first km equations of system (1) are determined:*

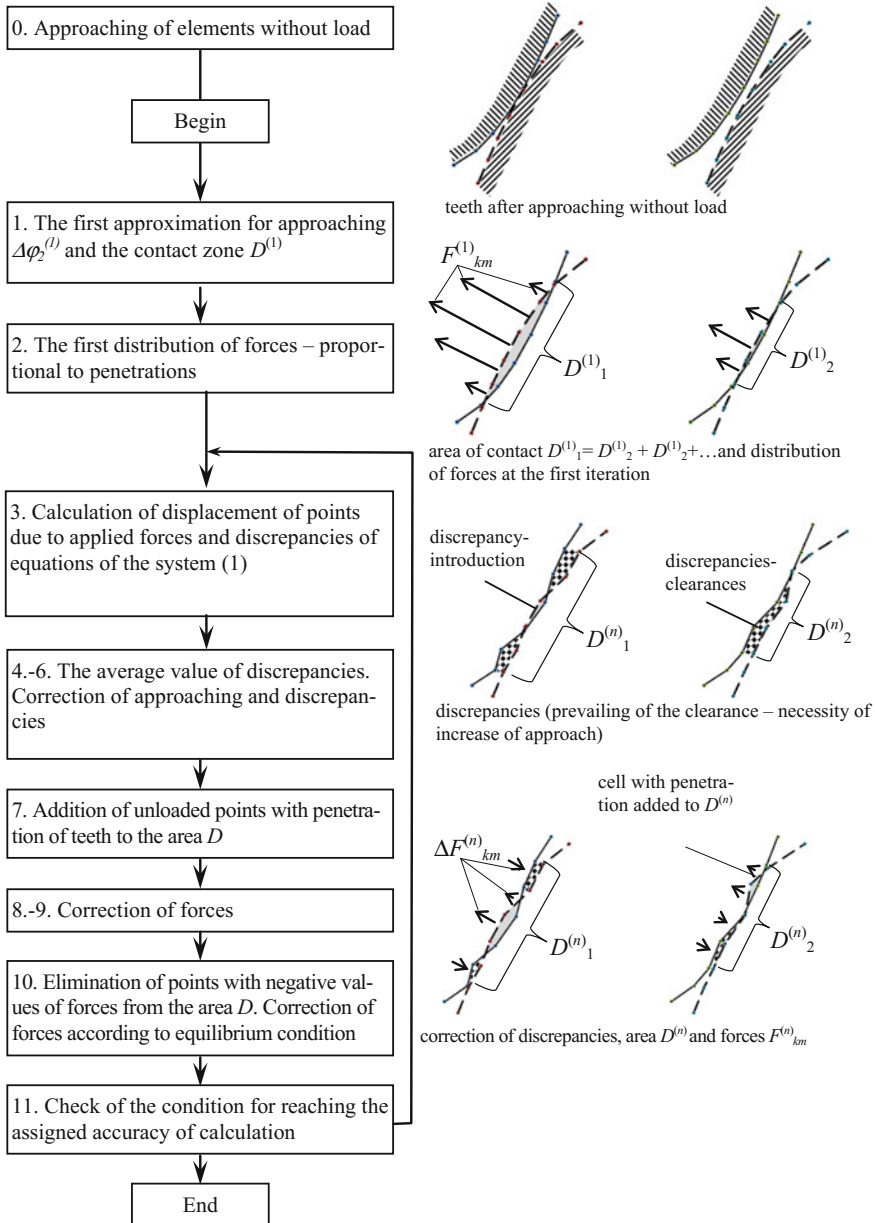


Fig. 2 Scheme of analysis of a multi-pair elastic loaded gear

$$w_{km} = \sum_D F_{k'm'} (v_{1km k'm'} + v_{2km k'm'}) = \sum_D F_{k'm'} v_{km k'm'}, \quad (4)$$

$$\xi_{km}^{(n)} = w_{km}^{(n)} + S_{0km} - \Delta\varphi_{2km}^{(n)}. \quad (5)$$

- (4) *The average value of discrepancies within the area D reduced to the angle of the gearwheel rotation is determined:*

$$\xi_{av}^{(n)} = \frac{1}{I} \sum_D \xi_{km}^{(n)} / r_{2km}. \quad (6)$$

- (5) *The chosen value of approaching $\Delta\varphi_2^{(n)}$ for the next $(n + 1)$ th iteration is corrected by the value of the average discrepancy:*

$$\Delta\varphi_2^{(n+1)} = \Delta\varphi_2^{(n)} + \xi_{av}^{(n)}. \quad (7)$$

- (6) *Discrepancies ξ_{km} are corrected for the new value of approaching $\Delta\varphi_2^{(n+1)}$:*

$$\tilde{\xi}_{km}^{(n)} = S_{0km} + w_{km}^{(n)} - \Delta\varphi_{2km}^{(n+1)} = \xi_{km}^{(n)} - \xi_{av}^{(n)} r_{2km}. \quad (8)$$

- (7) *The area D [the number km of equations of system (1)] is corrected. After correction of the value of approaching (7), those cells (unloaded at the nth iteration) should be added to area D, for which $\tilde{\xi}_{km}^{(n)} < 0$.*

- (8) *Corrections $\Delta F_{km}^{(n+1)}$ to discretely applied forces are determined. This is the crucial step of the algorithm. The manner of changing the values of forces determines the convergence of iteration to the solution. In our opinion, in order to correct the forces, it is reasonable to use the moments of discrepancies available at the moment. This issue will be considered in detail below.*

- (9) *Values of forces are determined at the following iteration:*

$$f_{km}^{(n+1)} = F_{km}^{(n)} + \Delta F_{km}^{(n+1)}. \quad (9)$$

- (10) *The area D is corrected again [the number km of equations of system (1)]. Cells with negative values of $f_{km}^{(n+1)}$ are excluded from it, while for the rest of the cells, the values of forces are corrected in accordance with the condition of their equilibrium:*

$$F_{km}^{(n+1)} = T_2 f_{km}^{(n+1)} / \sum_D f_{km}^{(n+1)} \tilde{r}_{2km}. \quad (10)$$

(11) *The condition of reaching the value of correction of forces (step 8) of the assigned allowable low value is checked. In the case of a negative result, we return to step 3.*

The end of the algorithm.

Let us consider the issue of the rational variation of values of discretely applied forces within iterations. In particular, we study the classical method for a simple iteration applied for solution of traditional large systems of linear equations (note that the “peculiarity” of our case is that the number of equations in (1) can, in general, be varied during analysis). Let us further assume conditionally that the first I equations of system (1) will be solved at each iteration, having represented it as

$$\mathbf{N} \cdot \mathbf{F} = \mathbf{b}, \quad (11)$$

where \mathbf{N} is the matrix of the influence factors, \mathbf{F} is the column vector of the sought-after, discretely applied forces, and \mathbf{b} is the column vector of free members of the system, its coordinates being the values $\Delta_{\varphi 2km} - S_{0km}$ (therefore, the value $\Delta_{\varphi 2km}$ is temporarily considered to be constant). Discrepancies in equations of system (11) should be reduced to a minimum. It should be accounted for that, in general, the matrix \mathbf{N} is unsymmetrical, since the compliance of various areas of teeth is different, for example, it is increased when approaching the edges (faces or apexes) of teeth and it is decreased closer to the recess (tooth root) [1, 2, 6], thus imposing limitations for choosing certain efficient methods of solution of such large systems of equations.

The method of simple iteration for solving system (11) implies its reduction to the form

$$\mathbf{F} = \mathbf{B} \cdot \mathbf{F} + \mathbf{c}. \quad (12)$$

In this case, the solution is found to be the limit of the sequence

$$\mathbf{F}^{(n+1)} = \mathbf{B} \cdot \mathbf{F}^{(n)} + \mathbf{c}. \quad (13)$$

In the simplest case, the basis for correction of \mathbf{F} can be the column vector $\boldsymbol{\xi}$ of discrepancies of Eq. (11) obtained at the previous iteration

$$\mathbf{F}^{(n+1)} = \mathbf{F}^{(n)} - t^{(n+1)} \boldsymbol{\xi}^{(n)} = \mathbf{F}^{(n)} - t^{(n+1)} (\mathbf{N} \cdot \mathbf{F}^{(n)} - \mathbf{b}). \quad (14)$$

Equation (14) is reduced to the form (13) if we accept that

$$\mathbf{B} = \mathbf{E} - t^{(n)}\mathbf{N}, \quad (15)$$

where \mathbf{E} is the unit matrix. In the general case, the scalar parameter $t^{(n)}$ can be replaced by the matrix $\mathbf{T}^{(n)}$ with the diagonal consisting of factors $t_{km}^{(n)}$ that are suitably chosen for the km th components of \mathbf{F} and the remaining cells are zero:

$$\mathbf{F}^{(n+1)} = \mathbf{F}^{(n)} - \mathbf{T}^{(n)} \cdot \xi^{(n)}. \quad (16)$$

Let us call the iteration process in which $t^{(n)}$ ($\mathbf{T}^{(n)}$) does not change at iteration a stationary one; otherwise, we deal with a non-stationary process.

The iteration process (14) can be given a reasonable physical essence: for the cells in which $\xi_{km}^{(n)} > 0$ (a clearance appeared at iteration), the increment of the force at the following iteration must be negative (the current value of the force causes too large a deformation, which is why a clearance appears); otherwise (if there is a penetration, that is, $\xi_{km}^{(n)} < 0$), the increment of the force must be positive. The iteration relations for the correction of forces proposed in [2, 11] can be reduced to the following form at the next iteration:

$$F_{km}^{(n+1)} = F_{km}^{(n)} - \frac{\tau_I}{\left(w_{km}^{(n)} + S_{0km}\right)} \xi_{km}^{(n)}, \quad (17)$$

$$F_{km}^{(n+1)} = F_{km}^{(n)} - \frac{\tau_{II}}{\sum_{k'm' \in D} v_{kmk'm'}} \xi_{km}^{(n)}. \quad (18)$$

We proposed the following, more simple and, as will be shown below, rather efficient iteration relation for the correction of forces:

$$F_{km}^{(n+1)} = F_{km}^{(n)} - \frac{\tau_{III}}{v_{km}} \xi_{km}^{(n)}, \quad (19)$$

factors τ/v_{km} of which are components of the vector of parameters $\mathbf{T}^{(n)}$. Another non-crucial correction that considers the feature of the algorithm stated above is introduced here: having defined the method for correcting the value of approaching $\Delta\varphi_2$ and the area D at the next iteration in steps 6, 7 and 8, it is better that we use the column vector $\tilde{\xi}$ of the corrected discrepancies (8).

The physical meaning of relation (19) can be explained as: the $(n+1)$ th increment of the force for compensation of “penetration” or “clearance” (appearing within the calculation at the n th iteration) depends on the elastic properties of the loaded system, that is, the more the system reacts to the change of load at this step (the factors of influence are greater at the denominator), the less the increment of the force must be.

We considered the convergence of the above given iteration algorithm for different parameters τ by the example of the conjugated spiroid gear of a heavy-loaded

low-speed gearbox with a loading torque of 2000 Nm. The basic parameters of the test gear are given in Table 1.

Figure 3 shows the diagrams of variation of numerical parameters of the analysis when applying relations (17)–(19) within the iteration cycle. As can be seen, the parameters can be arranged as follows with regard to the velocity of specification: approaching, discrepancies, discretely applied forces.

We considered the behavior of a stationary iteration process for different values of parameters τ . The main results are shown in Fig. 4. As was expected, when decreasing the values $\tau_{I,II,III}$, the velocity of convergence is decreased; and when the above given values are increased, the algorithm begins diverging—first locally and then, as a rule, globally.

As can be seen, the optimal parameter τ can have a very wide range of values. In this context, it is desirable to have a more versatile parameter that regulates the velocity of convergence. In order to get it, let us consider the possibilities of a non-stationary iteration process for which we will use information on the variation of discrepancies at the last iteration; namely, let us assume that:

- this variation depends on the parameter τ linearly:

$$\frac{\Delta \zeta_{\text{mean sq.}}^{\zeta(n)}}{\tau(n)} = \frac{\Delta \zeta_{\text{mean sq.}}^{\zeta(n+1)}}{\tau(n+1)}, \quad (20)$$

where $\Delta \zeta_{\text{mean sq.}}^{\zeta(n,n+1)} = \sqrt{\sum_{D^{(n)}} \left(\zeta_{km}^{(n-1,n)} - \zeta_{km}^{(n,n+1)} \right)^2 / N_D^{(n)}}$ is the mean square variation of discrepancies at the n th ($(n+1)$ th) iteration;

- there is a certain desired value of V of the relation. At first sight, it is desirable to assign a big relation, however, as the results shown in Fig. 5 prove, there is a certain improvement of system (1) that is limited for solution of the elastic system; and it is obtained at two neighboring iterations:

$$\xi_{km}^{(n+1)} = \xi_{km}^{(n)} / V. \quad (21)$$

Table 1 Basic parameters of the test gear

Center distance (mm)	60
Axial module of the worm (mm)	2.75
Gear ratio	46:1
External diameter of the spiroid worm (mm)	42
External/internal diameters of the spiroid gearwheel (mm)	175/138
Factors of the addendum/dedendum	1/1.2
Profile angles of the right/left flanks	10°/30°

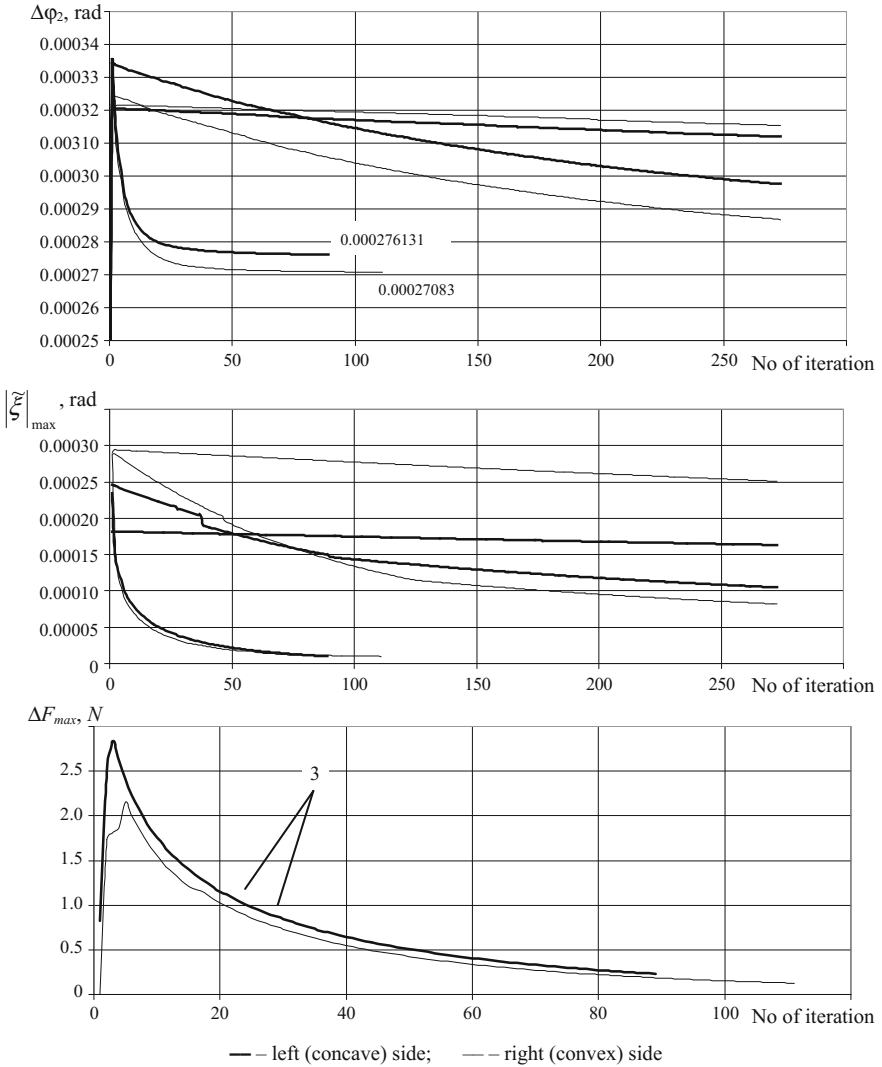


Fig. 3 Convergence of the algorithm for different iteration relations: 1, 2, 3 correction of forces with regard to (17–19), respectively

One can obtain, as a result,

$$\tau^{(n+1)} = \tau^{(n)} \left(1 - \frac{1}{V} \right) \frac{\zeta_{\text{mean sq.}}^{(n)}}{\Delta \zeta_{\text{mean sq.}}^{(n)}}. \quad (22)$$

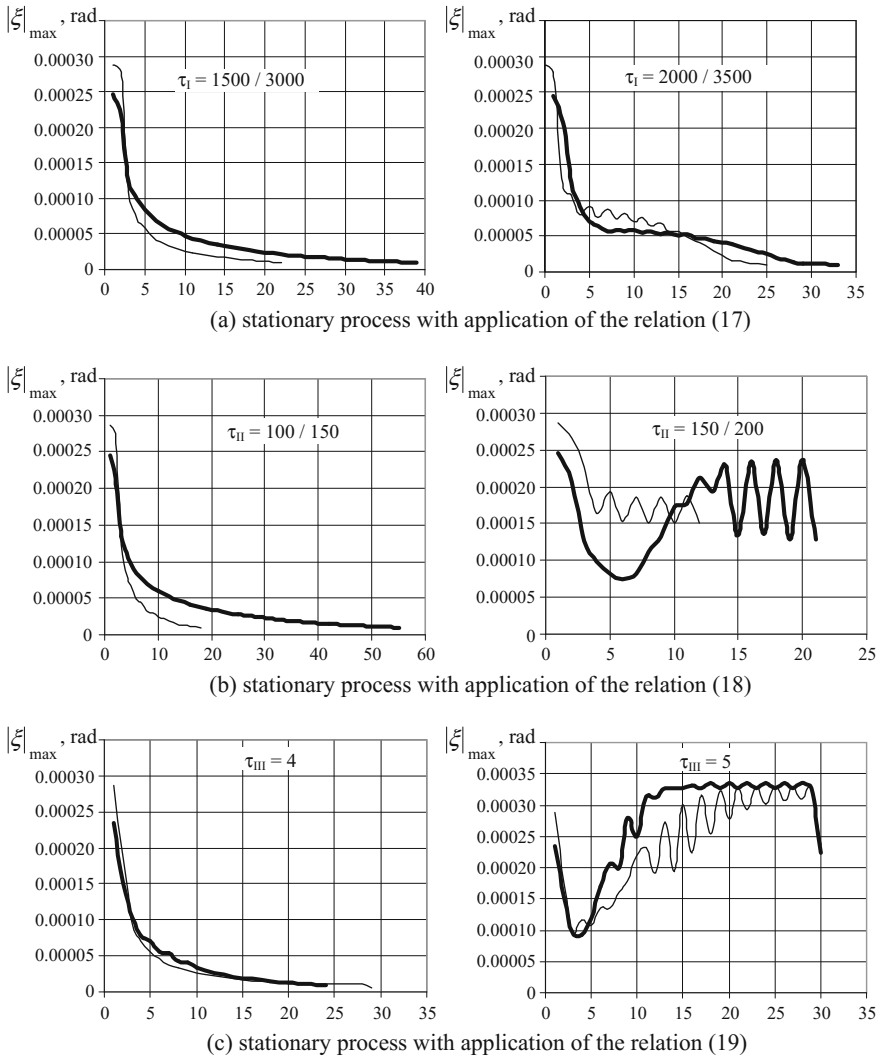


Fig. 4 Convergence of the algorithm for different parameters of τ (the nominator of the value is for the *left flank*, the denominator is for the *right flank*)

The efficiency of the applied procedure is illustrated by the results of the test calculations shown in Fig. 5. As can be seen, comparatively close optimal values of the parameter V are obtained: 1.6–1.8, providing, in this case and as a rule, better convergence than that for the stationary process.

Specific extrapolation (20) of the behavior of discrepancies at the n th iteration to the future behavior of discrepancies obtained at the $(n + 1)$ th iteration is a rather contradictory procedure. The greater the specification obtained at a certain iteration

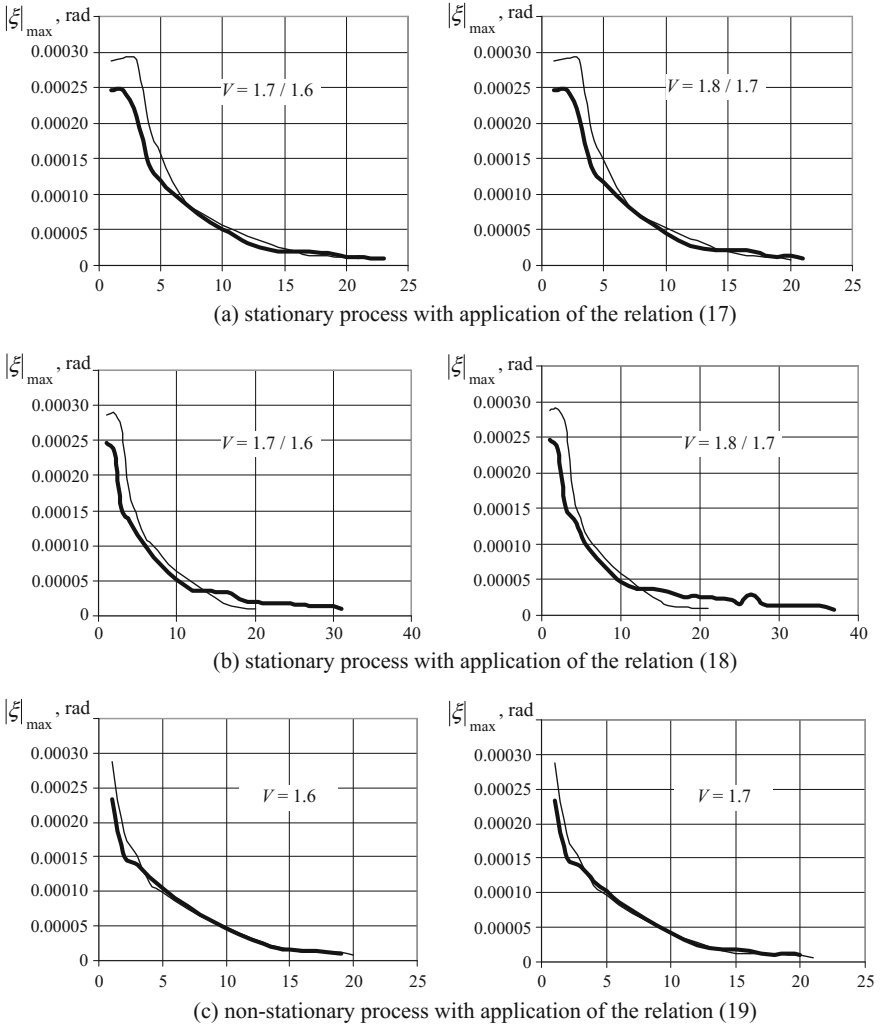


Fig. 5 Convergence of the algorithm of the parameter τ at regulation by (22)

(configuration of discrepancies will be changed more significantly, correspondingly), the less the expectation that the tendency obtained at this iteration will be further kept. No worse and sometimes better results can be obtained when performing the next but one iteration with small values of factors τ for more precise assessment of the velocity of convergence. Performance of these, at first sight, idle iterations allows for forecasting the behavior of discrepancies and, correspondingly, for succeeding in the velocity of convergence.

3 Assessment of the Influence Function of Teeth and Threads

As was stated above, the considered solution of the problem of searching for load distribution in the gearing is based on discretization of the elastic system, its equilibrium state being described by Eq. (1). An important component of the part of this system of equation which determines its solution and participates in implementation of the iteration algorithm is the influence function $v_{km\ k'm'}$. This function reflects the reaction of the position of cells that form a continuous flank of the tooth (thread) on the external action by the value of 1 N in one of them. Traditionally, two components of the influence function are singled out: contact and bending-and-shearing (here and further, the subscript 1 indicates the relation of the parameter to the worm thread, and the subscript 2 is for the gearwheel tooth):

$$v_{1,2} = v_{1,2}^k(\tilde{x}, \tilde{y}) + v_{1,2}^u(\tilde{x}, \tilde{y}). \quad (23)$$

Plotting of the influence functions has been performed within the coordinate systems shown in Fig. 6; for each of them, the counting of the tooth height is done along one of the coordinate axes, and the counting of the tooth length is done along the other one. The initial surface and its unfolding have a common point C which is the center of unfolding: for the gearwheel tooth, this point is at the intersection of the mean cylinder and the pitch surface of the gear rim; for the worm thread, it is at the pitch cylinder.

3.1 Contact Component of the Influence Function

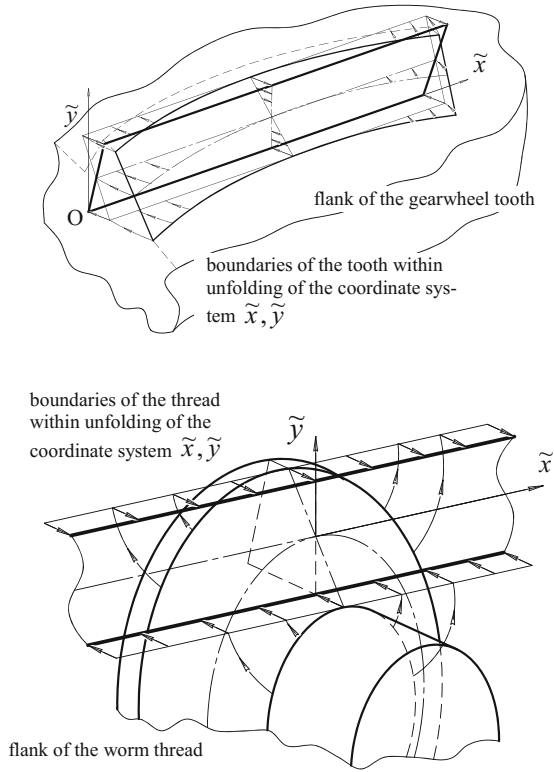
The classic solution of the problem of assessing the contact displacements at the point $i(x, y)$ due to the arbitrarily $k(x', y')$ applied unit normal force is the Boussinesq relation for the semi-space:

$$v(x, y) = \frac{\alpha}{r}, \quad r = \sqrt{(x - x')^2 + (y - y')^2}, \quad \alpha = \frac{1 - \mu^2}{\pi E}. \quad (24)$$

The main and obvious difficulty of applying this function within the following software implementation for the considered approach is the tendency of its value to infinity when considering the deformations in the vicinity infinitely close to the loading point.

The second feature of its application to the analysis of the loaded contact is that teeth have finite dimensions comparable with the dimensions of contact areas. That is why the influence function should additionally consider the closeness of the apex and face edges where the compliance is higher, and also recesses at their roots, where the compliance is conversely lower [10]. We have taken the solutions

Fig. 6 Coordinate systems for plotting the influence function



obtained in [2, 10] as the basis and augmented them with regard to peculiarities of the geometry of the spiroid gear:

$$v_1^k(\tilde{x}, \tilde{y}) = ((1 - \mu_1^2)/(2rE_1)) \cdot (B_1 + B_2 + B_8), \quad (25)$$

$$v_2^k(\tilde{x}, \tilde{y}) = ((1 - \mu_2^2)/(2rE_2)) \cdot \sum_{j=1}^8 B'_j, \quad (26)$$

$$\begin{cases} \text{for } r_j^2 \geq r^2 & B'_j = 1 - \frac{2}{\pi} \arctan\left(\sqrt{r_j^2/r^2 - 1}\right), \\ \text{for } r_j^2 < r^2 & B'_j = 1, \end{cases} \quad j = \overline{1, 7} \quad (27)$$

$$\begin{cases} \text{for } r_8^2 \geq r^2 & B'_8 = -1 + \frac{2}{\pi} \arctan\left(\sqrt{r_8^2/r^2 - 1}\right), \\ \text{for } r_8^2 < r^2 & B'_8 = -1, \end{cases}$$

$$\tilde{x}_{\min} = \tilde{y}_p \tan(\Psi), \quad (28)$$

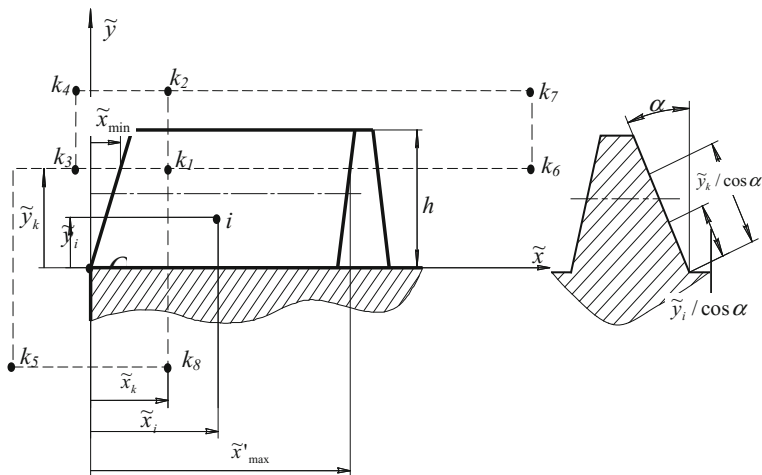


Fig. 7 Definition of contact displacement at the point i for load application at the point k on the gearwheel tooth flank

where r_j is the distance from the point i of the displacement measurement to the point k of load application ($j = 1$) and its j th mirror-like image given in Figs. 7 and 8, accounting for the oblique boundary of the tooth (\tilde{x}_{\min}).

Relations (26)–(28) given above allow for assessing the contact displacements with account for the closeness of the tooth and thread apices, their roots, and two faces of the tooth, one of them having massive basis outside the tooth (Fig. 9). Note here that, similar to the traditional procedure [2, 10, 13], we assume that the convexity (concavity) of the tooth flank does not influence the character of the contact deformations (at least within those tooth areas where these deformations are significant), and that the difference of angles between the tooth flanks on one hand and the faces, apices and root on the other hand, from the value of 90° , does not significantly influence the values and character of the contact deformations.

Fig. 8 Definition of contact displacement at the point i for load application at the point k on the flank of the spiroid worm thread

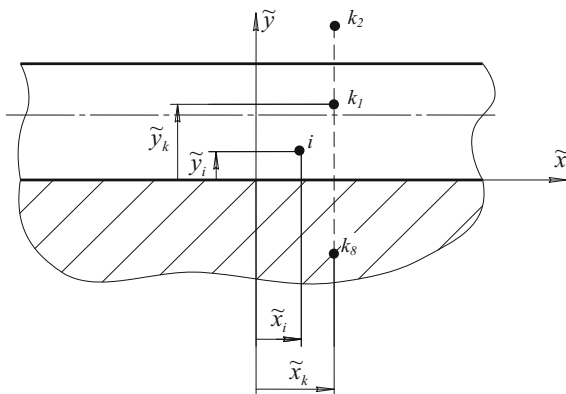
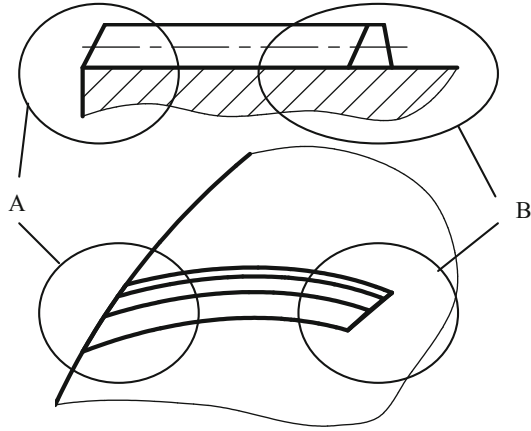


Fig. 9 Areas *A* and *B* of different rigidity of the tooth root



Accounting for the influence of both faces is necessary when the tooth length is less than 9 modules (the value is obtained on the basis of numerical research of tooth compliance); this is the length at which the tooth curvature can be neglected. In other cases, the factors B_1 , B_2 and B_6 or B_7 and B_8 should be excluded, depending on which of the faces ends up being closer to the considered point.

3.2 Influence Function of the Bending and Shearing Compliance

Prof. E. Airapetov proposed, in [1], the model of the bending displacement of teeth as being

$$w(x, y) = K(x) \cdot K(y), \tag{29}$$

where $K(y)$ is the function characterizing the variation of displacement (in this context) along the height; and $K(x)$ is the function characterizing the variation of displacement along the length (it is constructed on basis of the Fourier composition). After numerous experimental investigations in the field of gear couplings, planetary and double-enveloping worm gears, this method has been developed up to the discretely continuous model of the tooth with the elastic root. We have augmented this model with account for the tooth geometry features for a spiroid gear, and the model ended up taking the following form:

$$v_1'' = (h^3 \cos^2 \alpha / \pi D_1) k_{1x} k_y k_d, \tag{30}$$

$$v_2'' = (h^3 \cos^2 \alpha / \pi D_2) k_{2x} k_y k_l k_R, \tag{31}$$

$$\begin{cases} k_y = k_{y2} [1 + k_{y1} \tilde{Y}^2 (\tilde{Y}_k - \tilde{Y}_i/3)] & \text{for } 0 \leq \tilde{Y} \leq \tilde{Y}_k, \\ k_y = k_{y2} [1 + k_{y1} \tilde{Y}_k^2 (\tilde{Y}_i - \tilde{Y}_k/3)] & \text{for } \tilde{Y}_k \leq \tilde{Y} \leq 1 \end{cases}, \quad (32)$$

$$k_{1x} = e^{-\beta \Delta \tilde{X}} (\cos \beta \Delta \tilde{X} + \sin \beta \Delta \tilde{X}), \quad (33)$$

$$\begin{aligned} k_{2x} = & e^{-\beta \Delta \tilde{X}} (\cos \beta \Delta \tilde{X} + \sin \beta \Delta \tilde{X}) + k_{x1} e^{-\beta k_{x2} (\Delta \tilde{X} + \tilde{x}_k)} \cos \beta k_{x2} \Delta \tilde{X} \\ & + k_{x3} e^{-\beta k_{x4} (\Delta \tilde{X} + 2\tilde{x}_k)} \times [\cos \beta k_{x4} (\Delta \tilde{X} + 2\tilde{x}_k) - \sin \beta k_{x4} (\Delta \tilde{X} + 2\tilde{x}_k)], \end{aligned} \quad (34)$$

$$k_l = 1 + k_{l1} (h/l)^{k_{l2}}, \quad (35)$$

$$k_R = 1 - k_{R1} (S_{ef2}/R)^{k_{R2}}, \quad (36)$$

$$k_d = 1 + k_{d1} (h \cos \gamma_1 / d_{f1})^{k_{d2}} \quad (37)$$

$$\begin{aligned} \tilde{Y}_i &= \tilde{y}_i/h, \Delta \tilde{X} = |\tilde{X}_i - \tilde{X}_k| = |\tilde{x}_i - \tilde{x}_k|/h, \\ \tilde{Y}_k &= \tilde{y}_k/h, \tilde{X}_k = \tilde{x}_k/h, \end{aligned} \quad (38)$$

Relative dimensionless coordinates \tilde{X} and \tilde{Y} of the center of the cell i at which the displacement is calculated and cells k of force application are counted from the nearest face for a tooth and from the center of unfolding for a thread. The particular case of the factor k_d is its equality to 1 at an infinitely large diameter of the worm solid and the helix angle of the thread equal to 90° ; this corresponds to the problem of an infinitely long plate with an elastic root loaded by a concentrated force.

Numerical simulation has been carried out to specify the type of relation and numerical value of factors which are components of (30)–(38). Simulation was done using the finite element method, and it implied the consequent stamp loading of flanks at their different points, singling the results of contact components out of the obtained results, the components being calculated in accordance with relations (25)–(28), and the consequent approximation of the remaining bending and shearing displacements. An example of these calculation results at loading in the center of the tooth is given in Fig. 10. It was established after the simulation that:

- (1) as expected (see Fig. 9), the compliance of the “tooth heel” (the area adjacent to the external diameter of the gearwheel) is higher than the compliance at the center of the unfolding by a factor of 8 when loading along the left flank; and by a factor of 1.7 when loading along the right flank. These values for the “tooth toe” (the area adjacent to the internal diameter of the gearwheel) are 1.4 and 2.7, respectively (Fig. 11);
- (2) elastic displacements at thread flanks decrease down to small values at a distance $1/8$ – $1/4$ of the thread pitch (smaller values are for cases with big diameters of the worm solid);

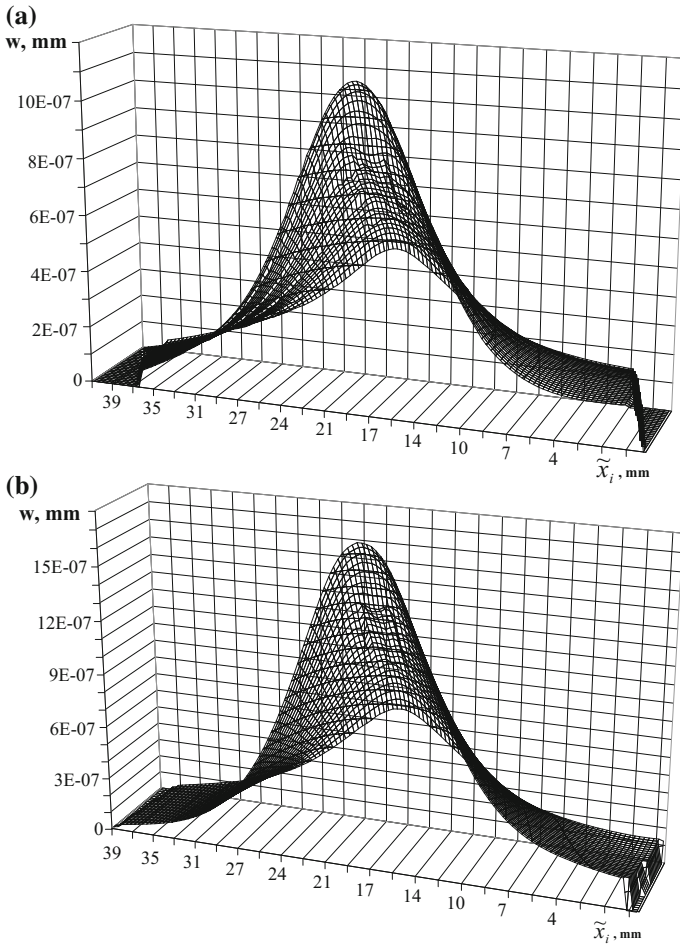


Fig. 10 Bending- and shearing displacements of a tooth when loading the left (a) and right (b) flanks at the center C of the tooth

(3) factors which are components of (28)–(36) have the following values (they turned out to be different for the opposite name flanks due to the asymmetry of teeth in a spiroid gear) for the gearwheel tooth:

$$k_{R1} = 10; k_{R2} = 2; S_{ef2} = 0.97 \cdot S_{f2} (S_{a2}/S_{f2})^{0.2};$$

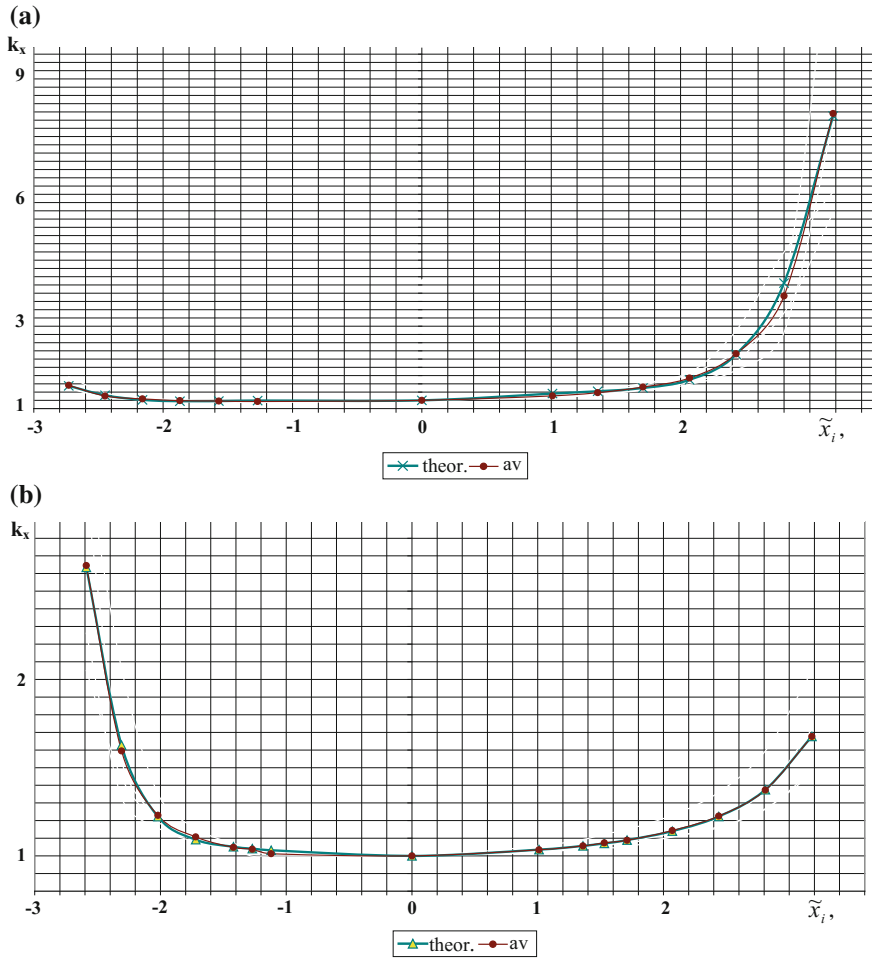


Fig. 11 Variation of the bending compliance along the tooth (loading of the left (a) and right (b) flanks)

– for the left loaded flank:

$$\beta = 1.18; k_{l1} = 18; k_{l2} = 3.2;$$

$$k_{y1} = 0.063 + 0.0733 \cdot \tilde{Y}_k; k_{y2} = 7.036 + 4 \cdot \tilde{Y}_k;$$

at the toe end:

$$k_{x1} = 4.86; k_{x2} = 2.08; k_{x3} = 1.4; k_{x4} = 1.2;$$

at the cap end:

$$k_{x1} = 0.11; k_{x2} = 0.25; k_{x3} = 1.5; k_{x4} = 1;$$

– for the right loaded flank:

$$\beta = 1.28; k_{l1} = 21; k_{l2} = 3.7;$$

$$k_{y1} = 0.061 + 0.0795 \cdot \tilde{Y}_k; k_{y2} = 7.742 + 1.87 \cdot \tilde{Y}_k;$$

– at the toe end:

$$k_{x1} = 1.25; k_{x2} = 0.9; k_{x3} = 2.1; k_{x4} = 1.9;$$

– at the cap end:

$$k_{x1} = 0.6; k_{x2} = 0.08; k_{x3} = 2.0; k_{x4} = 1.0.;$$

for the worm thread:

– for the left loaded flank:

$$\beta = 1.27; k_{y1} = 0.0632 + 0.1548 \cdot \tilde{Y}_k; k_{y1} = 10.124 - 1.9345 \cdot \tilde{Y}_k;$$

$$k_d = 1 + 3.7(h \cos(\gamma_1)/d_{f1})^2;$$

– for the right loaded flank:

$$\beta = 1.2; k_{y1} = 0.1206 + 0.1464 \cdot \tilde{Y}_k; k_{y1} = 9.408 + 2.2024 \cdot \tilde{Y}_k;$$

$$k_d = 1 + 2.9(h \cos(\gamma_1)/d_{f1})^2.$$

Note that application of the finite element analysis is preliminary, a sort of adjusting procedure; its results are valid for a variety of investigated gears, and the main algorithm for assessing the loading state of a multi-pair gear is carried out based on approximating relations.

4 Consideration of Plastic Deformations

First of all, we consider such a level of gear loading and such distribution of contact stresses (established after the first loading cycles) for which contact contortion is not continued (is not progressed). Evidently, a situation of the hyper-loading of a gear is possible when the loading torque and contact stresses are so high that contact contortion at the tooth flanks continues developing after each loading cycle (other fractures are also possible). Though this important case should be detected in calculations, our considered quantitative analysis of the loaded contact does not cover this case.

Putting it all aside, one can single out two statements of the problem of the loaded gear analysis:

- the geometry of the contact flanks is known, and such a load distribution is determined that provides conditions of equilibrium and displacement compatibility; this is practically the analysis of an elastically loaded gear in a pure form;
- load distribution is known; the geometry of the flanks is to be determined, providing conditions of equilibrium and displacement compatibility; it can be, for instance, synthesis of the tooth flanks in accordance with the assigned law of force distribution.

The considered problem of analysis of an elastic and plastic loaded gear is a sort of combination of these two problems: there are areas of elastic contact and areas of elastic-and-plastic contact in such a gear, for which the geometry of the flanks (plastic deformations) should be selected in accordance with the assigned limiting contact stress.

Four types of cell on the loaded teeth are singled out in a discretized model of a loaded gear:

- cells of the first type, in which stresses are so high that contact contortion covers these cells completely; one can consider that the initial micro-roughnesses become completely contorted in this case;
- cells of the second type, in which plastic deformation is specific only for apexes of micro-roughnesses;
- cells of the third type, for which the elastic deformation takes place;
- cells of the fourth type, which do not take part in load transfer.

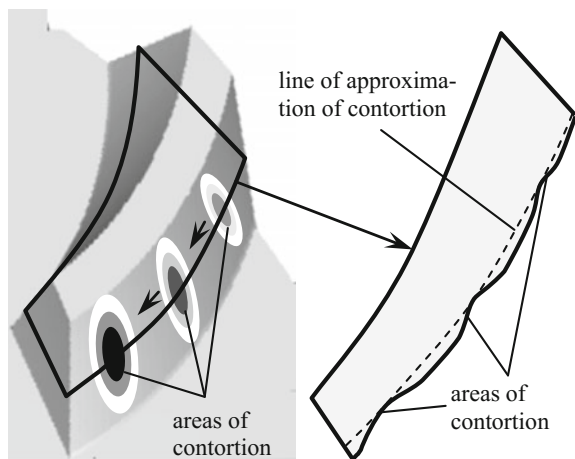
When loaded elements are rotating, the maximum part of the plastic deformation is displaced along the contact flanks, together with the contact areas, changing them irreversibly (changing the coordinates of points, “drowning” the points into the “tooth solid”). At the consequent loading cycles, the contact surfaces (that are the final object of analysis) will have this very state: changed not only close to the specific considered contact area, but also along the significant part of the tooth flank. That is why the first assessment of contortion cannot be precise: cells that are not contorted, or even loaded at this phase of meshing, will probably be among those contorted at the next phase when the contact area is displaced, with the

contorting load definitely appearing there. This consideration will certainly influence the stress distribution and, consequently, the conditions for the presence of contorted cells and the value of contortion in the analysis. Therefore, in order to specify the set of contorted cells and the values of the simulated contortion for them, another cycle of iterations (external with regard to the algorithm of the load distribution analysis) should be introduced; and it should be carried out after the analysis of load distribution along the whole flank of teeth and threads. Meeting these requirements means repetition of a relatively time-consuming analysis for a rather large (infinitely large at the extreme) number of meshing phases. An alternative can be consideration of a relatively small number of phases with the generation of contortion areas on tooth flanks (sets of points with coordinates being changed at simulation of contortion). After that, approximation of the maximum values of simulated contortions in cells can be carried out. Such an approach is demonstrated in Fig. 12.

Nevertheless, in our opinion, the additional external cycle of iterations is too time-consuming. Calculation of the plastic deformation of contact flanks can be added directly to the algorithm described above for load distribution analysis; in this case, the algorithm is supplemented with the following features (Fig. 13):

- after initial assessment (or beginning with a certain iteration, that is, after obtaining a rather precise distribution of forces) of the contact area, the value of elements approaching and the values of discretely applied forces, the type of each loaded cell is determined; for cells of the first type, the value of contortion is determined (see below);
- the following values are corrected in accordance with the values of discrepancies obtained at each consequent iteration:

Fig. 12 Approximation of plastic deformation on the tooth flank



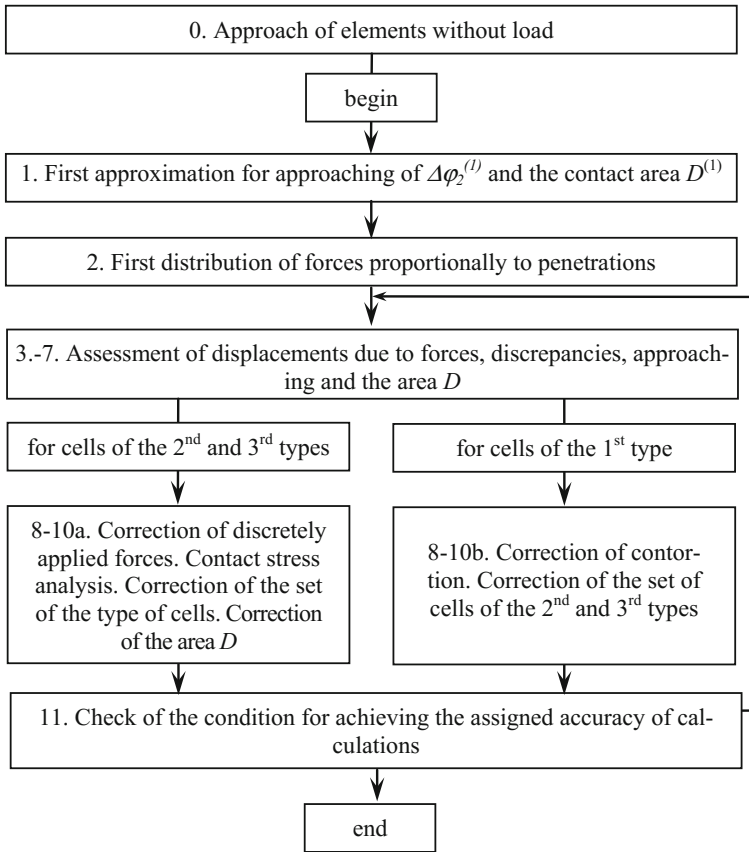


Fig. 13 Scheme of consideration of plastic deformations

for cells of the first type, the value of contortion;
 for cells of the second and third types, the values of forces;

– relation of the cell to one or another type can vary:

to contorted ones (type one), on exceeding the allowable limit of the design stress;
 to elastically deformed ones (types two and three), on achieving the negative value of contortion.

5 Simulation of Plastic Deformation of the Contact Surface Area (Cells of the 1st Type)

Here, we deal with cells of the 1st type; during calculations, the level of contact stress in them exceeded the assigned limit. The latter is often determined for contact in gears in accordance with the following relation:

$$[\sigma_h] = 2.8\sigma_T, \quad (39)$$

where σ_T is the yield point of the material.

It is reasonable to calculate the values of plastic displacement w_{pkm}^{n+1} and the force F_{km}^{n+1} applied at the overloaded km th cell at step 11, depending on the values obtained for this cell at the current n th iteration: elastic displacement w_{hkm}^n , acting σ_{hkm}^n and allowable $[\sigma_h]$ contact stresses:

$$w_{pkm}^{n+1} = w_{km}^n \left(1 - \frac{[\sigma_h]}{\sigma_{hkm}^n} \right), \quad (40)$$

$$F_{pkm}^{n+1} = F_{km}^n \frac{[\sigma_h]}{\sigma_{hkm}^n}. \quad (41)$$

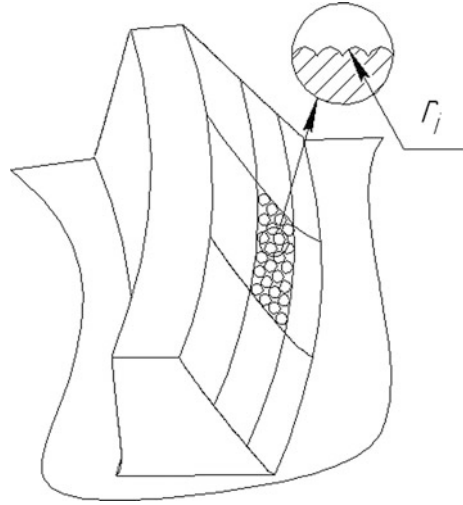
6 Simulation of Deformation of Micro-roughnesses

We accept for the cells of the 1st type that plastic deformation of micro-roughnesses is equal to the height of the profile relative to the mean line (R_p).

In order to calculate deformations of the micro-roughnesses of cells of the 2nd and 3rd types, a numerical model proposed by Izmailov [6] has been taken as the basis; we adapted it to our algorithm with the following features and allowances:

- (1) The tooth flank is represented as a certain number of micro-roughnesses in the form of segments of a sphere (see Fig. 14). The actual micro-relief of the surface, which is the alternation of ridges (marks of cuts at tooth machining), is surely different from such a model; however, as is shown in [7], the accepted allowance provides a rather satisfactory level of errors. Dimensions of segments (heights and radii) are random values, which are distributed in accordance with the two-parametrical beta-distribution. Parameters of beta-distribution are chosen based on relations [3, 9] that take into account the results of measurement of real rough surfaces. The dimensions of single recesses in each specific cell are the same, and their number depends on:
 - the dimension of the cell itself;
 - the radius and height of micro-roughnesses that are average for the tooth.

Fig. 14 Single recesses in the cell of the gearwheel tooth flank



The dimension of the cell is chosen so that it could fit at least one single recess.

(2) The force acting on the single recess is equal to

$$F_i = \frac{F_{km}}{n}, \quad (42)$$

where n is the number of single recesses in the given cell.

(3) Relation of cells to the 2nd or 3rd type is carried out based on the dimensionless coefficient α calculated by the formula

$$\alpha = \left(1 + \sqrt{\frac{F_{cr,i}}{F_i}} \right)^{-1}, \quad (43)$$

where $F_{cr,i}$ is the critical force calculated by the formula

$$F_{cr,i} = 14 \frac{H^3 r_i^2}{E^{*2}}, \quad (46)$$

where r_i is the radius of rounding of the single recess, E^* is the equivalent Young module, and H is the micro-hardness of the surface. For $\alpha < 0.5$, the contact is considered to be elastic, and the cell is related to the third type; for $\alpha = 0.5-1$, the contact is elastic and plastic, and the cell is related to the second type.

(4) Deformation in cells of the 2nd type is calculated by the formula

$$\delta_{n,i} = \delta_{cr,i} \left(0.5 \frac{F_i}{F_{cr,i}} + 0.5 \sqrt{\frac{F_i}{F_{cr,i}}} \right), \tag{47}$$

$$\delta_{cr,i} = 5 \frac{H^2 r_i}{E^{*2}}. \tag{48}$$

Deformation in cells of the 3rd type is calculated by the formula

$$\delta_{y,i} = \left(\frac{9}{16} \frac{F_i^2}{r_i E^{*2}} \right)^{\frac{1}{3}}. \tag{49}$$

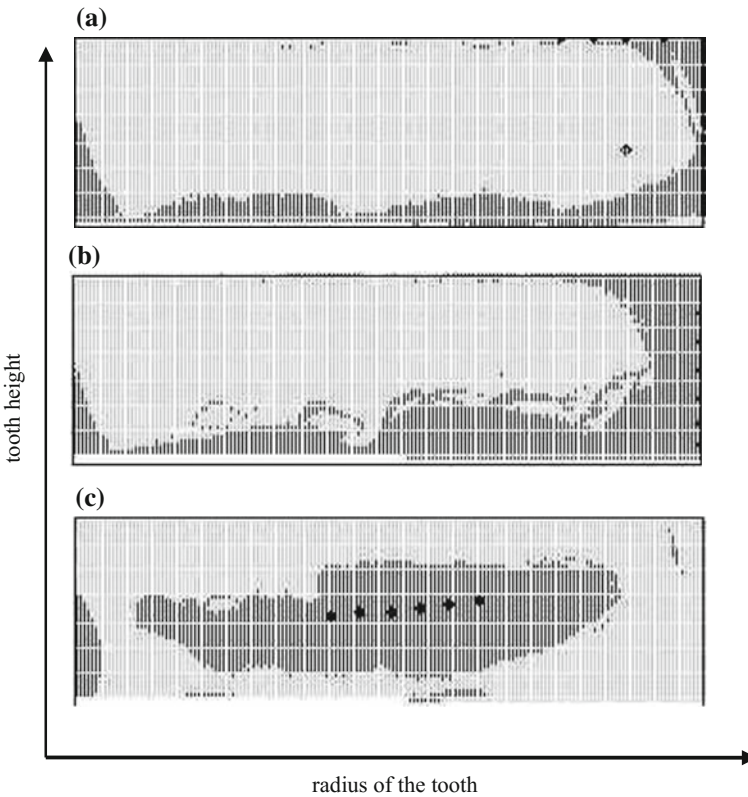


Fig. 15 Projection of the summarized contact pattern onto the axial plane of the gearwheel

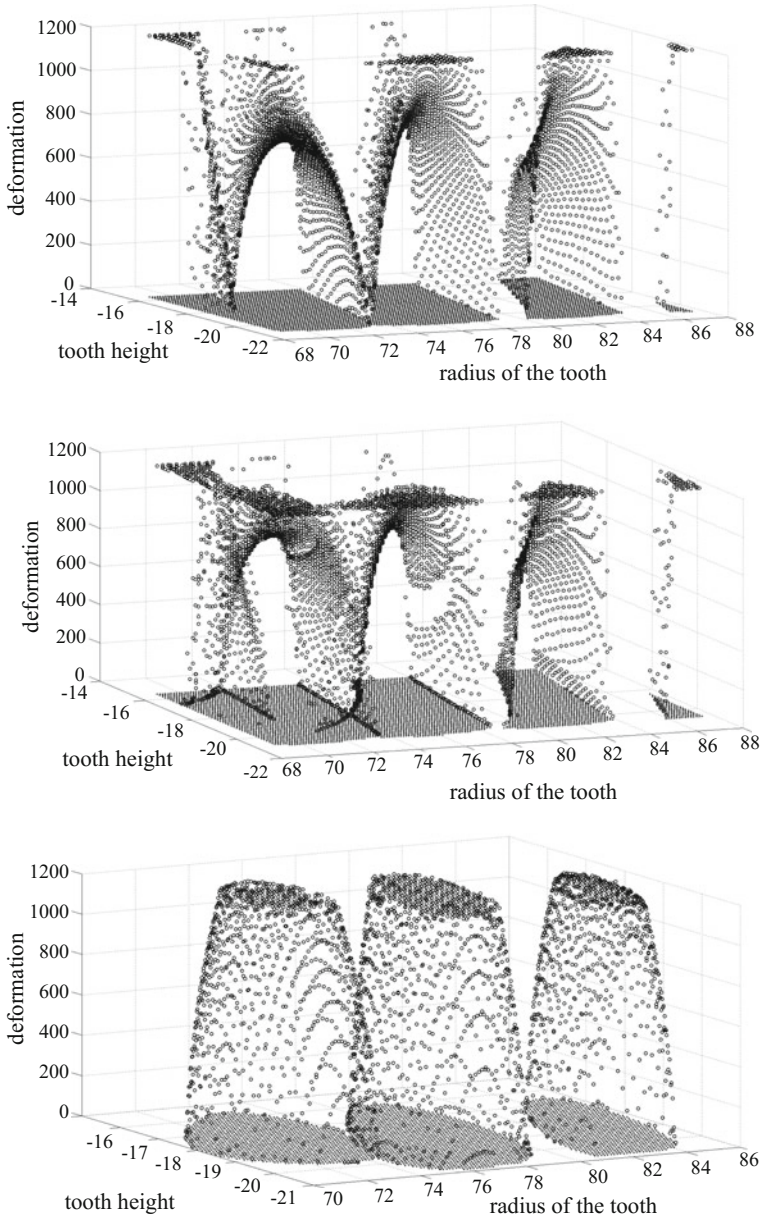


Fig. 16 Distribution of contact stresses along contact areas

7 Examples of Calculations

The example that illustrates the workability of the algorithm is shown in Figs. 15 and 16; several results of calculating the loading of a gear with parameters are given in Table 1 for the loading torque of 4000 Nm and an allowable level of contact stresses at the gearwheel of 1200 MPa. In particular, these Figs. show the summarized contact patterns on the left (concave) tooth flanks in projections on the axial plane of the gearwheel with shadowing of areas subjected to plastic deformation, and the corresponding three-dimensional diagrams of distribution of contact stresses along the contact areas obtained at one meshing phase and conditionally projected onto the flank of one tooth, for the cases:

- of the conjugated contact in the absence of errors (Figs. 15a, and 16a);
- of the conjugated contact accounting for the increased compliance of the gearwheel and worm units (this corresponds approximately to the error of the interaxial angle in a gear 0.1/30) (Figs. 15b, and 16b);
- of the contact which is localized along the tooth height and length (Figs. 15c, and 16c).

In all the cases, the summarized contact pattern is propagated along the entire active tooth flank. The maximum of plastic deformation in a conjugated gear is at the edges of the teeth, a tendency that is strengthened when introducing the errors. Consideration of plastic deformations provides an increase in the area of each individual contact area by 10–12% on average.

8 Conclusions

The algorithms of analysis of load distribution in multi-pair spiroid gearing described in the paper can be applied for both the elastic and elastic-and-plastic statements of the problem. The algorithms are adjusted for high productivity and validity of calculations in accordance with the results of numerical and real experiments. Calculation results are applicable for assessment of the tooth strength of heavy-loaded gears.

References

1. Airapetov, E., Genkin, M., Melnikova, T.: Statics of Double-Enveloping Worm Gears. M., Nauka (1981) (in Russian)
2. Bondarenko, A.: Static loading of double-enveloping worm gearing with account of features of generation, manufacture and assembly errors, compliance of gear elements. PhD Thesis, Kurgan (1987) (in Russian)

3. Demkin, N.: Multi-level models of friction contact. *Trenie i iznos*, **21**(2), 115–120 (2000) (in Russian)
4. Hohn, B., Steingrover, K., Lutz, M.: Determination and optimization of the contact pattern of worm gears. *Proceedings of the International Conference on Gears VDI* **1**, 341–352 (2002)
5. Houser, D.: The effect of manufacturing microgeometry variations on the load distribution factor and on gear contact and root stresses. *Gear Technol.* **6**, 51 (2009)
6. Izmailov, V., Chaplygin, S.: Numerical and analytical simulation of discrete contact of machine parts. *Naukovedeniye* **6** (2014) <http://naukovedenie.ru/PDF/10TVN614.pdf> (in Russian)
7. Izmailov, V., Kurova, M.: Application of beta-distribution for analysis of contact of rough solids. *Treniye i iznos* **IV**(6), 983–990 (1983) (in Russian)
8. Moriwaki, I., Watanabe, K., Nishiwaki, I., Yatani, K., Yoshihara, M., Ueda, A.: Finite element analysis of gear tooth stress with tooth flank film elements. In: *Proceedings of the International Conference on Gears VDI*, pp. 39–63 (2005)
9. Ogar, P., Tarasov, V., Maksimova, O.: Contacting of a rough surface through the layer of viscous elastic coating. In: *Proceedings of the V International Conference “Problems of mechanics of advanced machines”*, Ulan-Ude (2012) (in Russian)
10. Sheveleva, G.: Analysis of elastic contact displacements on surfaces of parts with limited dimensions. *Mashinostroeniye* **4**, 92098 (1984) (in Russian)
11. Sheveleva, G.: Numerical method for solution of the contact problem at compression of elastic solids. *Mashinovedeniye* **5**, 90–94 (1981) (in Russian)
12. Sheveleva, G.: Solution of the contact problem by method of consequent loading. *Izvestiya vuzov, Mashinostroeniye* **9**, pp. 10–15 (1986) (in Russian)
13. Zablonsky, K.: *Gears. Load distribution in meshing*. K., Tekhnika (1977) (in Russian)